Rapid Deglacial Response of the Laurentide Ice Sheet during the Allerød Warm Interval Through the High Peak Wilderness of the Adirondack Mountains, New York, USA

Barker, K., Barth, A.M., Cuzzone, J.K., Hidy, A.

Supplemental Materials

Section 1. Model analysis of deglacial patterns

We calculate the simulated deglaciation age across the Adirondack domain (Figure S1). The resulting pattern reveals a clear south-to-north retreat occurring between ~13.5 and 12 kyr BP, with spatial heterogeneity in timing that suggests the influence of additional processes, including topography. To isolate the dominant large-scale pattern of ice retreat, we fit a least-squares planar surface to the deglaciation timing field as a function of latitude. This planar fit represents the first-order spatial gradient in retreat timing (Figure S1C), capturing the regional-scale structure independent of local variability. The residual (Figure S1D), computed as the difference between the deglaciation age and the fitted trend, highlights deviations from this large-scale pattern.

The residual field reveals systematic, spatially coherent departures from the latitudinal retreat trend that closely correspond with underlying topography (Figure S1A). Regions of delayed deglaciation relative to the large-scale gradient are concentrated in higher-elevation areas, including the High Peaks Area (HPA), whereas earlier-than-expected retreat occurs in lower-elevation and more peripheral regions. This indicates that local topographic controls modulate the timing of retreat beyond the first-order spatial gradient.

Elevation-binned analysis further supports this interpretation. Median deglaciation timing increases with elevation, confirming a strong hypsometric control on retreat, consistent with reduced ablation and enhanced ice persistence at higher elevations. The residual–elevation relationship (Figure S1E) shows that these deviations are also systematically related to elevation, with higher-elevation regions exhibiting later-than-expected deglaciation by up to ~200 years (median). Together, these results indicate that while large-scale deglaciation across the High Peaks region was primarily governed by ice margin retreat, ice surface thinning contributed to earlier exposure of high-elevation summits relative to adjacent lower-elevation valleys. However, consistent with geochronological constraints, ice margin retreat across this region was rapid (~500 years), and the influence of ice thinning on the overall deglaciation pattern was marginal.

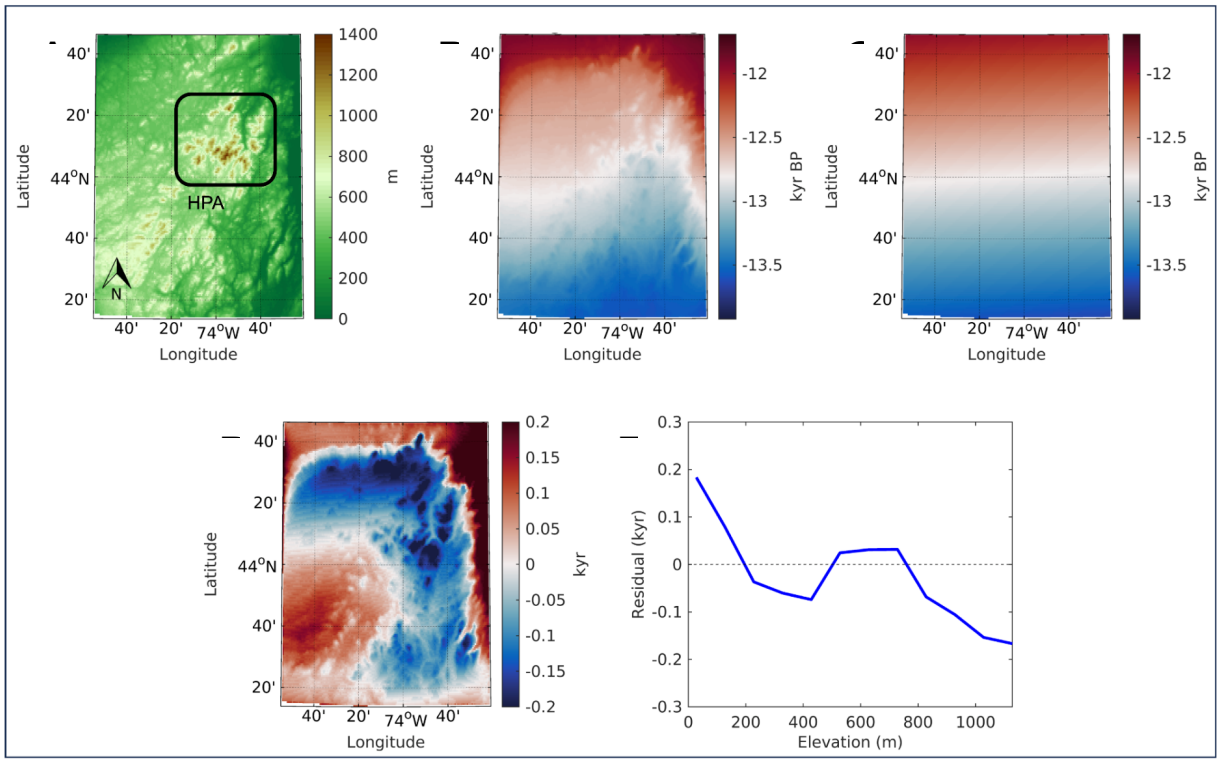


Figure S1. Timing of simulated deglaciation by elevation across the ADK region. (a) Bedrock elevation across the ADK model domain, with the High Peaks Area (HPA) outlined. (b) Simulated deglaciation age across the model domain. (c) Fitted spatial trend in modeled deglaciation age, representing the first-order regional pattern of ice-margin retreat from south to north. (d) Residual deglaciation timing after subtracting the fitted regional trend from the modeled deglaciation-age field (B - C). Residuals therefore show locations that deglaciated earlier or later than expected from the regional retreat pattern alone. Blue indicates earlier deglaciation, and red later deglaciation. (e) Median residual deglaciation age binned by bedrock elevation. After removal of the regional retreat trend, the highest elevations deglaciate up to ~0.4 kyr earlier than surrounding lower-elevation terrain.

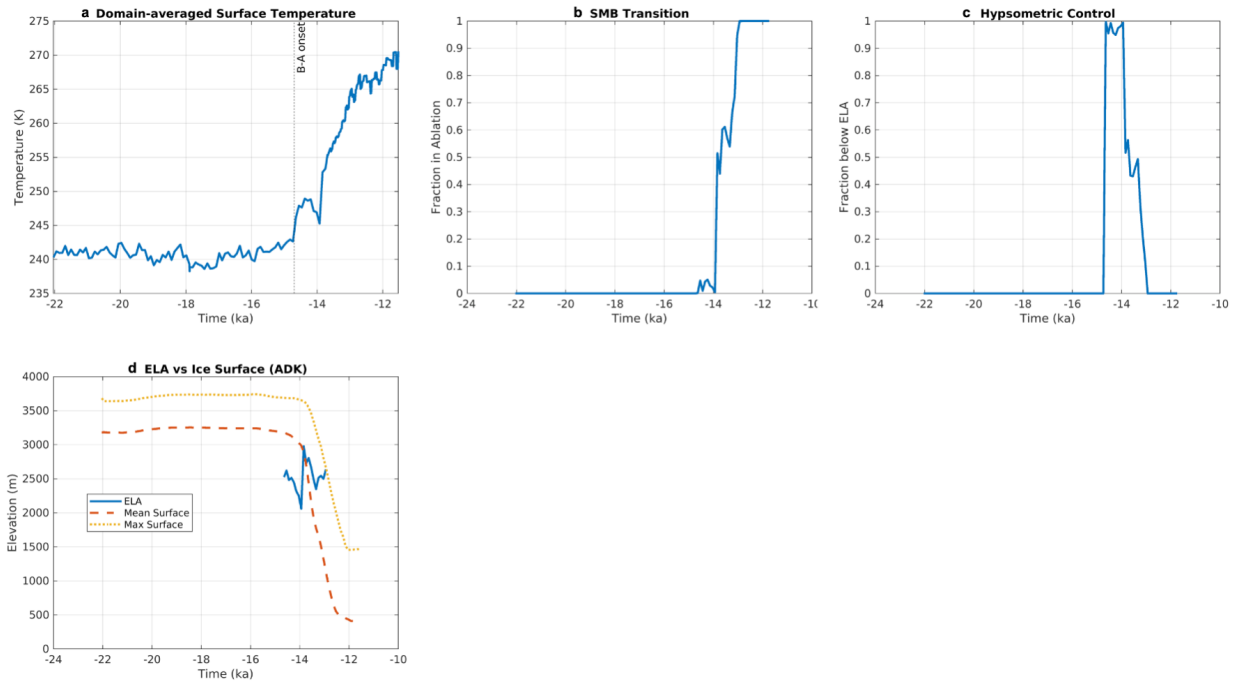


Figure S2. Transient ice sheet simulations of surface mass balance and equilibrium line altitude. (a) Domain-averaged surface temperature (K) through time (dashed line indicates the Bølling-Allerød onset). (b) Fraction of ice-covered nodes experiencing net ablation (surface mass balance < 0), illustrating a rapid transition from predominantly accumulation to widespread ablation at ~14 ka. (c) Fraction of ice-covered area below the equilibrium line altitude (ELA). (d) Evolution of ELA (solid blue) relative to mean (dashed) and maximum (dotted) ice surface elevation across the model domain.

Section 2. Model analysis of deglacial mechanisms

The temporal evolution of surface temperature, equilibrium line altitude (ELA), and surface mass balance (SMB) provide further insight into the mechanisms controlling deglaciation (Figure S2). Domain-averaged surface temperature increases at the onset of the Bølling–Allerød ~14.7 ka, accelerating at ~14 ka, after which a more rapid warming occurs coincident with the onset of deglaciation. This transition is accompanied by a sharp increase in the fraction of the domain experiencing net ablation. The relationship between ELA and ice surface elevation highlights the role of hypsometry in modulating this transition. Prior to ~14 ka, the ELA remains well below both the mean and maximum ice surface elevations, allowing the ice sheet to persist across most of the domain. As warming accelerates, the ELA rises rapidly and intersects the ice surface, first approaching the mean elevation and then the highest elevations within the domain. This intersection coincides with a brief interval in which a large fraction of the domain lies near the ELA, as reflected in the hypsometric control metric. During this period, small changes in ELA produce large changes in the fraction of the ice sheet undergoing ablation, amplifying mass loss and accelerating retreat.

This transient alignment between ELA and ice surface elevation provides a mechanistic explanation for the rapid (~500 year) deglaciation observed in both the model and geochronological constraints. Together, these results indicate that while the spatial pattern of deglaciation is governed by large-scale retreat, the rate of retreat is strongly controlled by a response in SMB driven by the rise of the ELA through the ice sheet hypsometry.

Table S1 - Major element chemistry for samples analyzed for cosmogenic 36Cl

Sample Name	Al_2O_3 %	CaO %	Fe_2O_3 %	K_2O %	MgO %	MnO %	Na_2O %	P_2O_5 %	SiO_2 %	TiO_2 %	V_2O_5 %	Cr_2O_3 %	LOI
BB-22-02	25.15	11.51	0.00	1.01	0.05	0.00	4.33	0.00	57.88	0.08	0.00	0.00	0.00
BB-22-05	24.82	9.82	5.97	1.06	0.77	0.07	4.48	0.08	51.57	0.26	0.01	0.00	-0.03
BXR-22-02	20.92	9.17	6.44	1.57	2.00	0.09	3.65	0.00	55.66	0.49	0.00	0.00	0.00
BXR-22-03	24.48	10.30	4.57	0.98	1.37	0.06	4.26	0.19	52.20	0.47	0.01	0.01	0.14
BXR-22-05	17.62	11.05	12.80	1.39	2.31	0.20	2.85	3.54	43.83	1.32	0.01	0.00	2.62
HOP-22-01	21.21	5.91	0.00	4.08	0.00	0.00	5.44	0.00	63.28	0.07	0.00	0.00	0.00
HOP-22-04	18.71	7.33	10.40	2.14	1.86	0.16	3.69	0.49	52.50	1.49	0.01	0.00	0.26
LOM-22-02	25.83	9.51	3.79	0.89	0.93	0.04	4.47	0.06	53.24	0.23	0.01	0.00	0.52
PM-23-01	24.11	9.21	0.05	1.29	0.00	0.00	5.01	0.00	60.21	0.11	0.00	0.01	0.00
PM-23-02	21.73	8.96	5.99	1.77	0.95	0.10	4.68	0.28	54.65	0.89	0.00	0.00	0.00
WF-22-01	23.88	8.78	0.00	2.59	0.00	0.00	4.80	0.00	59.90	0.05	0.00	0.00	0.00
WF-22-03	23.11	10.55	5.41	0.84	2.71	0.07	4.01	0.10	51.22	0.45	0.01	0.01	1.15

All major element chemistry and LOI is listed in weight percent and was performed with X-ray fluorescence with 0.01% detection limit

Table S2 - Trace element chemistry for samples analyzed for cosmogenic 36Cl

Sample name	B (ppm)	Sm (ppm)	Gd (ppm)	U (ppm)	Th (ppm)	Cr (ppm)	Li (ppm)	Cl (ppm)
BB-22-02	10.0	0.6	0.3	0.1	0.3	210.0	10.0	3.6
BB-22-05	10.0	2.1	2.0	0.4	0.6	24.0	10.0	19.5
BXR-22-02	10.0	4.9	5.1	0.4	0.6	200.0	20.0	91.3
BXR-22-03	10.0	2.3	2.2	0.4	1.1	91.0	10.0	296.8
BXR-22-05	10.0	18.3	16.3	0.6	1.4	11.0	10.0	1.0
HOP-22-01	10.0	0.3	0.3	1.4	0.7	155.0	10.0	11.4
HOP-22-04	10.0	15.3	12.7	1.4	3.2	32.0	30.0	18.8
LOM-22-02	10.0	1.4	1.4	0.2	0.6	58.0	10.0	81.7
PM-23-01	10.0	0.4	0.3	0.2	0.2	153.0	10.0	7.9
PM-23-02	10.0	2.3	3.0	0.1	0.2	149.0	10.0	15.9
WF-22-01	10.0	0.2	0.2	0.3	0.3	149.0	20.0	25.5
WF-22-03	10.0	3.1	3.0	0.5	1.6	106.0	20.0	157.9

Trace elements were analyzed by ICP-MS with detection limits (ppm) as follows: 10 for B, Cr, Li; 0.1 for Sm, Th; 0.05 for Gd, U

Table S3 - Exposure age sensitivity tests for multiple erosional rates

	Erosion rate 0 mm kyr^{-1}			Erosion rate 1 mm kyr^{-1}			Erosion rate 5 mm kyr^{-1}		
Sample name	Age (ka)	Int. unc. (ka)	Tot. unc. (ka)	Age (ka)	Int. unc. (ka)	Tot. unc. (ka)	Age (ka)	Int. unc. (ka)	Tot. unc. (ka)
BB-22-02	11.8	0.5	0.9	11.9	0.5	0.9	12.3	0.6	1.0
BB-22-05	13.4	0.4	1.0	13.4	0.4	0.9	13.7	0.4	1.1
BXR-22-02	16.9	0.4	1.6	16.6	0.5	1.7	16.0	0.5	1.8
BXR-22-03	19.5	0.9	3.3	18.5	0.9	3.2	16.5	0.7	2.8
BXR-22-05	9.7	0.4	0.7	9.8	0.4	0.7	10.1	0.4	0.6
HOP-22-01	11.9	0.3	0.7	11.9	0.3	0.7	12.3	0.3	0.8
HOP-22-04	14.1	0.4	0.8	14.2	0.4	0.8	14.6	0.4	1.0
LOM-22-02	13.9	0.9	1.8	13.6	0.9	1.7	12.9	0.9	1.7
PM-23-01	12.4	0.4	0.7	12.5	0.4	0.8	12.8	0.4	0.8
PM-23-02	23.2	0.6	1.4	23.4	0.6	1.4	24.6	0.7	1.7
WF-22-01	15.1	0.4	1.0	15.1	0.3	0.8	15.3	0.3	1.2
WF-22-03	24.5	0.9	3.4	23.4	0.8	3.2	21.3	0.8	3.2